2021 International Conference on Unmanned Aircraft Systems (ICUAS)
Athens, Greece. June 15-18, 2021

Fast Adaptive Complementary Filter for Quadrotor Attitude Estimation During Aggressive Maneuvers

Rui Peng and Peng Lu

***Abstract*—It is challenging to provide accurate attitude estimation for a quadrotor during aggressive maneuvers, which involve violent and fast motion with uncertainty on sensors. In this unique case, we propose a fast adaptive Complementary Filter, which fuses raw measurements from a MARG sensor system and could cope with the large range of quadrotor manuvers. The performance of the filter is validated on an actual quadrotor platform, by comparing with the Extended Kalman Filter (EKF) and the Error State Kalman Filter (ESKF) simultaneously. The experimental results show that the proposed CF has better estimate accuracy, low time-latency and stable orientation outputs in a quadrotor's attitude estimate.**

I. Introduction

Aggressive maneuvers of Unmanned Aerial Vehicles (UAVs) are dominantly triggered by large-scale attitude changes or fast moves. Unlike smooth flights of UAVs in open environments, the aggressive maneuvers have the advantage of coping with flying through complex and constrained scenarios. Thus, applications for UAVs could be extended to agile obstacle avoidance, narrow-space exploration and inspection, or human-rescue under emergent situations.

With extensive efforts on state estimation, motion control and trajectory planning, an aerial robot is capable of addressing extreme flight conditions. [1] conducted aggressive flights with a quadrotor, which could be maintaining in a well-predicted state. The authors address the stabilization problem of hovering after a flip maneuver in [2]. Without a motion capture system, [3] proposes a quadrotor only equipped with a single camera and IMU for aggressive flights. The previous works [4]–[7] focus on motion-related solution, instead of the basic perspective: attitude estimation when a quadrotor engages in aggressive maneuvers. It is essential to accurately estimate the attitude for a quadrotor, during any moment of a flight. Generally, MARG sensors composed of a 3-axis MEMS gyroscope, an accelerometer and a magnetometer are considerably implemented on light-weight UAVs.

Categorized into two main sorts: Complementary Filter [8]–[10] and Kalman Filter [11]–[13], sensor fusion methods are widely considered to achieve a reliable solution. The fundamental principle of the CF is that the gyroscope and the accelerometer with the magnetometer compensate mutually, under different frequency domains. An issue of the CF is that it requires a proper filter gain to realize better performance of the attitude estimation. Among nonlinear filters, the the Extended Kalman Filter (EKF) is the most widely used. It uses Taylor-series expansion to linearize the nonlinear model, and then utilizes Kalman Filter for attitude estimation [14]. Unlike direct operation of the EKF, the Error State Kalman Filter (ESKF) [15] derives optimal attitude error which is based on measurements of sensors, to update current attitude with Kalman Filter.

The authors are with the Department of Mechanical Engineering, The University of Hong Kong. (Email: lupeng@hku.hk).

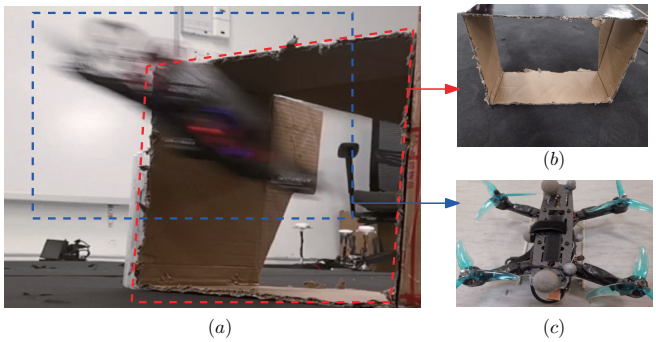

Fig. 1. The proposed quadrotor is flying through a narrow tunnel. (a) The aggressive and fast flight of the quadrotor. (b) An experimental box with a narrow tunnel. (c) Our quadrotor platform.

The above sensor fusion approaches are mostly well-performed and extensively implemented in many quadrotor platforms. However, iterative algorithms (KF) including matrix operation, take up much computation consumption. Also, their attitude estimation under circumstances of considerable self-acceleration and external magnetic distortion is not always reliable. The main contributions of this paper are listed as follows:

1) Aimed at accurate attitude estimate under large vibrations of the sensor body frame, we plan consecutive aggressive maneuvers (in Fig. 1) for a light-weight quadrotor to execute, under a motion capture system VICON.
2) Meanwhile, we propose a fast adaptive Complementary Filter for attitude estimation of the quadrotor, and it introduces a CF gain which is adaptively associated with sensors' outputs.
3) We compare the proposed CF with EKF and ESKF simultaneously, where results show that the CF has better estimate accuracy, low time-latency and stable estimate outputs.

The structure is arranged as following: Section II gives the brief system modeling for a quadrotor. Section III involves the details of the proposed fast adaptive CF. Section IV contains the experimental setup and results. Concluding insights are given in Section V.

2021 International Conference on Unmanned Aircraft Systems (ICUAS) | 978-1-6654-1535-4/21/$31.00 ©2021 IEEE | DOI: 10.1109/ICUAS51884.2021.9476796

II. System Modeling

In this section, we discuss sensor measurement models, UAV attitude representation system and dynamics of quadrotor maneuvers, which are basic for derivation of the proposed filter.

A. MARG Sensor Error Model

During aggressive flights, it is fundamental to ensure that the measurement data inputted into the sensor-fusion process, has high reliability. For a quadrotor, its MARG sensors provide raw measurements of the body frame with acceleration, magnetic field and angular velocity. The angular velocity obtained by the gyroscope, is modeled as:

$$\omega_m = \widetilde{\boldsymbol{\omega}}_r + \boldsymbol{b}_g + \boldsymbol{\mu}_g \tag{1}$$

where $\boldsymbol{\omega}_m$ is the measured angular velocity and $\widetilde{\boldsymbol{\omega}}_r$ is the real angular velocity. $\boldsymbol{b}_g$ and $\boldsymbol{n}_g$ are the random measurement bias of the gyro, and zero-mean gaussian white noise.

Subsequently, acceleration and magnetic field measurements are modeled by:

$$\begin{aligned} \boldsymbol{\alpha}_m &= \boldsymbol{R}^T(\widetilde{\boldsymbol{\alpha}}_r - \boldsymbol{g}) + \boldsymbol{b}_a + \boldsymbol{\mu}_a \\ \boldsymbol{m}_m &= \boldsymbol{R}^T(\widetilde{\boldsymbol{m}}_r - \boldsymbol{m}) + \boldsymbol{b}_m + \boldsymbol{\mu}_m \end{aligned} \tag{2}$$

where $\boldsymbol{\alpha}_m$, $\widetilde{\boldsymbol{\alpha}}_r$, $\boldsymbol{m}_m$ and $\widetilde{\boldsymbol{m}}_r$ represent the measured acceleration, ideal acceleration, measured magnetic field and ideal magnetic field, respectively. Similar to gyroscope, $\boldsymbol{b}_a$ and $\boldsymbol{b}_m$ denote the inherent sensor measurement bias of the accelerometer and magnetometer, with gaussian white noises: $\boldsymbol{\mu}_a$ and $\boldsymbol{\mu}_m$. Here $\boldsymbol{R}^T$ is the rotation matrix aligned with the quadrotor body frame and the inertial frame. The North-East-Down (NED) frame is established by $\boldsymbol{g} = [0 \quad 0 \quad 1]^T$ and $\boldsymbol{m} = [m_N \quad 0 \quad m_D]^T$, which are normalized gravitational acceleration in the world frame and magnetic field in inertial frame.

The accelerometer and magnetometer suffer from large-scale vibrations, which leads to relatively low reliability when the two sensors contribute to attitude estimation. In this case, the gyroscope provides high-frequency of angular rate, which compensate significantly. Therefore, to estimate gyro bias is the vital part to make the angular rate measurement accurate. On the other hand, during aggressive maneuvers, it is necessary to define an available status for acceleration and magnetic field to rectify error drift of the gyroscope.

B. Attitude Representation Model

Each quadrotor owns its rigid parameters and dynamic model, which allows us to define a determined attitude representation. Usually Euler angles: $\mathbf{RPY}$ are used to describe an orientation of a quadrotor. Here we define the quadrotor body frame as $\boldsymbol{B}$, and the inertial frame as $\boldsymbol{N}$. The Direction Cosine Matrix (DCM) for the transformation from $\boldsymbol{N}$ to $\boldsymbol{B}$ is denoted by $\boldsymbol{R}_N^B$, which is shown in Eq. (4) in terms of the orientation quaternion.

Furthermore, a normalized quaternion is utilized to represent the quadrotor's orientation during the sensor fusion computation. The quaternion describing attitude of the body frame relative to the world reference frame, could be defined as:

$$\boldsymbol{Q} = [q_w \quad q_x \quad q_y \quad q_z]^T, \quad ||\boldsymbol{Q}||^2 = 1 \tag{3}$$

where q_w is the scalar part and $\boldsymbol{q} = [q_x \quad q_y \quad q_z]^T$ is the rotation vector part of the quaternion. Additionally, the DCM is built by quaternion components:

$$\boldsymbol{R}_N^B = \begin{bmatrix} C_1 & 2(q_xq_y - q_wq_z) & 2(q_xq_z + q_wq_y) \\ 2(q_xq_y + q_wq_z) & C_2 & 2(q_yq_z - q_wq_x) \\ 2(q_xq_z - q_wq_y) & 2(q_yq_z + q_wq_x) & C_3 \end{bmatrix} \tag{4}$$

where $\begin{bmatrix} C_1 \\ C_2 \\ C_3 \end{bmatrix} = \begin{bmatrix} 1-2(q_y^2+q_z^2) \\ 1-2(q_x^2+q_z^2) \\ 1-2(q_x^2+q_y^2) \end{bmatrix}$. Then, the related Euler angles from the DCM terms are established by:

$$\begin{bmatrix} \phi \\ \theta \\ \psi \end{bmatrix} = \begin{bmatrix} \arctan(2(q_yq_z + q_wq_x)/(1-2(q_x^2+q_y^2))) \\ -\arcsin(2(q_xq_z - q_wq_y)) \\ \arctan(2(q_xq_y + q_wq_z)/(1-2(q_y^2+q_z^2))) \end{bmatrix}. \tag{5}$$

The attitude of a quadrotor in format of Euler angles will be employed in performance validation of the proposed filter, in aggressive maneuvers experiments.

C. Dynamic Model

To ensure the quadrotor maneuvers follow predefined trajectories, we implemented the property of differential flatness for the standard dynamic model:

$$\begin{aligned} m\ddot{\boldsymbol{l}} &= mg\boldsymbol{z}_W - \epsilon\boldsymbol{z}_B \\ \dot{\boldsymbol{\omega}} &= \boldsymbol{J}^{-1}[-\boldsymbol{\omega} \times \boldsymbol{J}\boldsymbol{\omega} + \boldsymbol{M}] \end{aligned} \tag{6}$$

where differential flatness of the quadrotor model was explained in [3]. In Eq. (6), $\boldsymbol{l}$ is the position vector of the quadrotor in the world reference frame, $\boldsymbol{\omega}$ is the angular velocity vector in the quadrotor body frame, and ϵ and $\boldsymbol{M}$ are the net thrust and moments in the quadrotor body frame. $\boldsymbol{J}$ and m are the inertia and mass of the quadrotor. $\boldsymbol{z}_B$ is the unit vector aligned with the axis of the four rotors and indicates the direction of thrust, while $\boldsymbol{z}_W$ is the unit vector denoting the direction of gravity.

An arbitrary trajectory segment is composed of four polynomial variables: a cartesian point x, y, z, and a heading orientation: ψ (yaw angle), which form two transient states in the world reference frame. The quadrotor flight controller is employed to execute maneuver trajectories, with individual outputs of thrust ϵ and moments $\boldsymbol{M}$ for four desired motor speeds:

$$\begin{aligned} \epsilon &= (-k_x\boldsymbol{e}_x - k_v\boldsymbol{e}_v + mg\boldsymbol{z}_W + m\ddot{\boldsymbol{l}}_d) \cdot \boldsymbol{R}\boldsymbol{z}_W \\ \boldsymbol{M} &= -k_R\boldsymbol{e}_R - k_\omega\boldsymbol{e}_\omega + \omega \times \boldsymbol{J}\omega - \boldsymbol{J}(\hat{\omega}\boldsymbol{R}^T\boldsymbol{R}_d\omega_d - \boldsymbol{R}^T\boldsymbol{R}_d\dot{\omega}_d) \end{aligned} \tag{7}$$

where $\boldsymbol{e}_x$, $\boldsymbol{e}_v$, $\boldsymbol{e}_R$, and $\boldsymbol{e}_\omega$ are the error vectors of position, velocity, orientation and angular rate. k_x, k_v, k_R, and k_ω are related control gains, and $\boldsymbol{R}$ is the rotation matrix denoting the orientation of the quadrotor, relative to the world reference frame. The subscript d indicates desired values.

III. Designed Filter

A. Orientation From Angular Velocity

A tri-axis gyroscope of the MARG system is used to provide high-frequency angular rates related to the x, y and z axes of the quadrotor's body frame ($\boldsymbol{B}$), referred as ω_x, ω_y and ω_z respectively. We use a 3-D vector to arrange the gyro-parameters in Eq. (8). The derivative of a quaternion indicates angular rate of change of the body frame relative to the world reference frame ($\boldsymbol{W}$). In Eq. (9), the dot product denotes the multiplication of a matrix and a vector, and the superscript $\hat{}$ denotes a normalized unit.

$$ {}^{B}\boldsymbol{\omega} = [\omega_x \quad \omega_y \quad \omega_z]^T \tag{8} $$

$$ {}^{B}_{W}\dot{\boldsymbol{q}} = {}^{B}\boldsymbol{\Omega} \cdot {}^{B}_{W}\hat{\boldsymbol{q}} \tag{9} $$

$$ {}^{B}\boldsymbol{\Omega} = \frac{1}{2}\begin{bmatrix} 0 & \omega_x & -\omega_y & -\omega_z \\ \omega_x & 0 & \omega_z & -\omega_y \\ \omega_y & -\omega_z & 0 & \omega_x \\ \omega_z & \omega_y & -\omega_x & 0 \end{bmatrix}. \tag{10} $$

The orientation of the earth frame relative to the sensor frame at time t, $\boldsymbol{q}_{\boldsymbol{\omega},t}$ can be computed by numerically integrating the quaternion derivative $\dot{\boldsymbol{q}}_{\boldsymbol{\omega},t}$ as described by Eq. (9), given that initial conditions are determined. In these equations, ${}^{B}\boldsymbol{\omega}_t$ is the angular rate vector measured at time t, Δt is the sampling period and $\boldsymbol{q}_{\boldsymbol{\omega},t-1}$ is the estimate of orientation at the last sampling time. The subscript $\boldsymbol{\omega}$ indicates that the quaternion is calculated from angular rates.

At any time t, the orientation of the quadrotor body frame under the world reference frame is denoted by ${}^{B}_{W}\boldsymbol{q}_{\boldsymbol{\omega},t}$, with the derivative of quaternion ${}^{B}_{W}\dot{\boldsymbol{q}}_{\boldsymbol{\omega},t}$. With known initial condition of the quadrotor's orientation, the relation between ${}^{B}_{W}\boldsymbol{q}_{\boldsymbol{\omega},t}$ and ${}^{B}_{W}\dot{\boldsymbol{q}}_{\boldsymbol{\omega},t}$ is established as:

$$ \begin{aligned} {}^{B}_{W}\dot{\boldsymbol{q}}_{\boldsymbol{\omega},t} &= {}^{B}\boldsymbol{\Omega}_t \cdot {}^{B}_{W}\hat{\boldsymbol{q}}_{est,t-1} \\ {}^{B}_{W}\boldsymbol{q}_{\boldsymbol{\omega},t} &= {}^{B}_{W}\hat{\boldsymbol{q}}_{est,t-1} + \int {}^{B}_{W}\dot{\boldsymbol{q}}_{\boldsymbol{\omega},t}\Delta t \end{aligned} \tag{11} $$

where ${}^{B}\boldsymbol{\Omega}_t$ as the orthogonal matrix of ${}^{B}\boldsymbol{\omega}_t$ is denoted in Eq. (10)

B. Orientation From Gravity And Magnetic Field

From the perspective of the gravity field ($\boldsymbol{G}$), a derivation of the auxiliary quaternion ${}^{G}\boldsymbol{q}_{\boldsymbol{\alpha}}$, is provided from acceleration ${}^{B}\boldsymbol{\alpha}$ and gravitation ${}^{G}\boldsymbol{g}$. With observation of the gravity vector in the world reference frame and the quadrotor body frame, the quaternion which realizes rotation transformation between two above frames is determined. Thus, the transformation between acceleration and gravitation could be built as:

$$ \boldsymbol{R}({}^{B}_{G}\boldsymbol{q})^{G}\boldsymbol{g} = {}^{B}\boldsymbol{a} \tag{12} $$

An element of the gravity vector in the world reference frame, is only related to the z-axis. Therefore, any rotation of the body frame about the z-axis could not bring any change to it. As a result, Eq. (12) is rewritten as:

$$ \boldsymbol{R}(\boldsymbol{q}_{\boldsymbol{\alpha}})\begin{bmatrix} 0 \\ 0 \\ 1 \end{bmatrix} = \begin{bmatrix} {}^{B}\alpha_x \\ {}^{B}\alpha_y \\ {}^{B}\alpha_z \end{bmatrix}. \tag{13} $$

By expanding Eq. (13), the transformation is further established as:

$$ \begin{bmatrix} 2(q_{\boldsymbol{\alpha},x} \cdot q_{\boldsymbol{\alpha},z} + q_{\boldsymbol{\alpha},w} \cdot q_{\boldsymbol{\alpha},y}) \\ 2(q_{\boldsymbol{\alpha},y} \cdot q_{\boldsymbol{\alpha},z} + q_{\boldsymbol{\alpha},w} \cdot q_{\boldsymbol{\alpha},x}) \\ q^2_{\boldsymbol{\alpha},w} - q^2_{\boldsymbol{\alpha},x} - q^2_{\boldsymbol{\alpha},y} + q^2_{\boldsymbol{\alpha},z} \end{bmatrix} = \begin{bmatrix} {}^{B}\alpha_x \\ {}^{B}\alpha_y \\ {}^{B}\alpha_z \end{bmatrix}. \tag{14} $$

However, the above system has infinite solutions, owing to the representation without any rotation about the z-axis (yaw). Hence, we implement definite roll and pitch angles with undetermined yaw angle, which leads to restriction of solutions. Then, $q_{\boldsymbol{\alpha},z}$ = 0 is made to simplify the system Eq. (14). For convenience, the solution with positive quaternion scalar (q_w) is employed to compute consequent quaternion from the gravity field:

$$ {}^{B}_{W}\boldsymbol{q}_{\boldsymbol{\alpha}} = \begin{bmatrix} \mu & -\dfrac{{}^{B}a_y}{2\mu} & \dfrac{{}^{B}a_x}{2\mu} & 0 \end{bmatrix}^T, \quad \mu = \sqrt{\frac{{}^{B}a_z + 1}{2}} \tag{15} $$

Then, according to Eq. (5), we can compute the roll and pitch angle of the quadrotor: $\phi_{\boldsymbol{\alpha}}$ and $\theta_{\boldsymbol{\alpha}}$. The subscript $\boldsymbol{\alpha}$ indicates the Euler angles are derived from acceleration.

To calculate the undefined yaw angle: ψ, we implement magnetometer outputs: ${}^{B}\boldsymbol{m} = [{}^{B}m_x \quad {}^{B}m_y \quad {}^{B}m_z]^T$, when the quadrotor is during flights and its body frame is not stationary. According to $\boldsymbol{m}^B = \boldsymbol{C}^B_W|_{\psi=\psi_{\boldsymbol{\alpha},\boldsymbol{m},W}} \cdot \boldsymbol{m}^W$, the transformation system could be extended to:

$$ \begin{aligned} {}^{B}m_x \cos\theta_{\boldsymbol{\alpha}} + {}^{B}m_y \sin\theta_{\boldsymbol{\alpha}} \sin\phi_{\boldsymbol{\alpha}} + {}^{B}m_z \sin\theta_{\boldsymbol{\alpha}} \cos\phi_{\boldsymbol{\alpha}} \\ = m_N \cdot \cos\psi_{\boldsymbol{\alpha},\boldsymbol{m},W} \\ {}^{B}m_y \cos\phi_{\boldsymbol{\alpha}} - {}^{B}m_z \sin\phi_{\boldsymbol{\alpha}} = -m_N \cdot \sin\psi_{\boldsymbol{\alpha},\boldsymbol{m},W} \end{aligned} \tag{16} $$

where ${}^{B}\boldsymbol{m} = [m_N \quad 0 \quad m_D]^T$ when the world reference frame coincides with the quadrotor body frame. Consequently, the heading angle $\psi_{\boldsymbol{\alpha},\boldsymbol{m},W}$ from both acceleration and magnetic field is obtained:

$$ \psi_{\boldsymbol{\alpha},\boldsymbol{m},W} = (-1)\cdot \arctan\left(\frac{{}^{B}m_y \cos\phi_{\boldsymbol{\alpha}} - {}^{B}m_z \sin\phi_{\boldsymbol{\alpha}}}{{}^{B}m_x \cos\theta_{\boldsymbol{\alpha}} + {}^{B}m_y \sin\theta_{\boldsymbol{\alpha}} \sin\phi_{\boldsymbol{\alpha}} + {}^{B}m_z \sin\theta_{\boldsymbol{\alpha}} \cos\phi_{\boldsymbol{\alpha}}}\right) \tag{17} $$

C. Fusion Strategy

In practice, initial attitude estimation could be obtained by the accelerometer and magnetometer, when the quadrotor is stationary. Due to drift error of gyroscope and unreliable measurement of the accelerometer during consecutive aggressive maneuvers, it is unreasonable to separate them in individual cases. The goal of the proposed fusion approach is to estimate a correct orientation where ${}^{B}_{W}\boldsymbol{q}_{\boldsymbol{\omega},t}$ is utilized to reduce high-frequency errors in ${}^{B}_{W}\boldsymbol{q}_{est,t}$, and ${}^{B}_{W}\boldsymbol{q}_{\boldsymbol{\alpha},\boldsymbol{m},t}$ is used to smooth integral drift errors of the gyroscope.

The mutual compensation in frequency domain ensures convergence of attitude estimate from initial conditions.

However, aggressive flights introduce more violence and intervention to the quadrotor MARG sensor system, with higher dynamic properties and wider orientation changes. It leads to limited range of estimation outputs from a conventional static Complementary Filter (CF) gain, established as:

$$ {}^{B}_{W}\boldsymbol{q}_{est,t} = \hat{\lambda}\,{}^{B}_{W}\boldsymbol{q}_{\boldsymbol{\alpha},\boldsymbol{m},t} + (1-\hat{\lambda})\,{}^{B}_{W}\boldsymbol{q}_{\boldsymbol{\omega},t}, \quad 0 \le \hat{\lambda} \le 1 \quad (18) $$

Hence, we introduce an adaptive CF gain to enhance the fusion performance, for addressing the filter dynamic insufficiency.

In terms of MARG sensors, angular rates $\boldsymbol{\omega}$ describe the extent of aggressive flights. When $\boldsymbol{\omega}$ tends to be zero, the estimate from accelerometer and magnetometer owns high credibility. In this case, $\hat{\lambda}$ in Eq. (18) is supposed to be low, to ensure ${}^{B}_{W}\boldsymbol{q}_{\boldsymbol{\alpha},\boldsymbol{m},t}$ takes up more proportion in orientation estimate. In the other hand, the quadrotor with high angular rates relies on ${}^{B}_{W}\boldsymbol{q}_{\boldsymbol{\omega},t}$. Therefore, we establish a relation between ${}^{B}_{W}\boldsymbol{q}_{\boldsymbol{\omega},t}$ and ${}^{B}_{W}\boldsymbol{q}_{\boldsymbol{\alpha},\boldsymbol{m},t}$ to optimize out an appropriate $\hat{\lambda}$, for determining respective filter gain weight.

We focus on heading angles from both ${}^{B}_{W}\boldsymbol{q}_{\boldsymbol{\omega},t}$ and ${}^{B}_{W}\boldsymbol{q}_{\boldsymbol{\alpha},\boldsymbol{m},t}$. In any sampling time period Δt of a flight, the integral of ω_z could be regarded as reference of the yaw angle: $\psi_{\boldsymbol{\omega},i}$, and $\psi_{\boldsymbol{\alpha},\boldsymbol{m},i}$ is taken as the divergent yaw angle. Then, to minimize the deviation, an adaptive filter gain $\hat{\gamma}_t$ at the time stamp t is built as:

$$ \hat{G}_t = \underset{\hat{\gamma}_t}{argmin} \sum_{i}^{n} \left(\psi_{\boldsymbol{\omega},i} - \psi_{\boldsymbol{\alpha},\boldsymbol{m},i}\right)^2 \quad (19) $$

where n denotes nearest sampling time periods. $\hat{\gamma}_t$ changing with time, is firmly binding with attitude estimate from MARG sensors, and it is affected by realtime dynamic status of the quadrotor. Therefore, we replace the $\hat{\lambda}$ in equa. (18) as $\hat{\gamma}_t$ to form the final proposed CF. The overview structure of the fusion strategy is shown as Fig. 2.

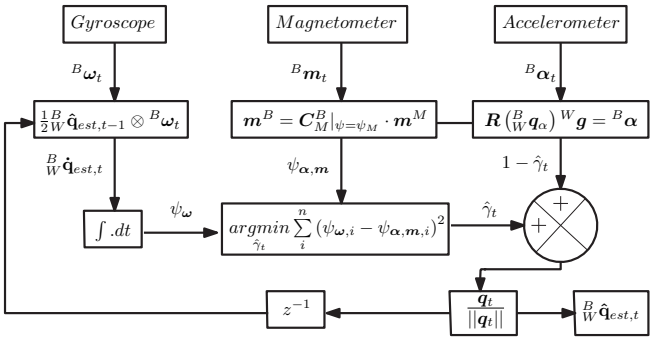

Fig. 2. Block diagram representation of the proposed adaptive Complementary Filter.

IV. Results

We use an indoor UAV flight-experiment field, which includes a motion capture system: VICON with 14-cameras. The VICON provides high accuracy of pose measurement for a rigid object, which is taken as ground-truth in algorithm validation. In experiments, we design three sorts of maneuvers: two-point loop maneuver, two-triangle loop maneuver and fixed-point rotation maneuver. To validate performance of the proposed CF, a light-weight quadrotor is implemented to execute aggressive maneuvers. During the maneuvers, we compare currently popular sensor fusion algorithms for attitude estimation: EKF (Extended Kalman Filter) and ESKF (Error State Kalman Filter) with the designed filter, in estimation of attitude Euler angles and runtime of a single algorithm epoch. Their stability of realtime estimate outputs is also considered.

A. Experimental Setup

The quadrotor platform uses QAV250 mechanism structure with limited weight and size. A Pixracer R15 flight controller is employed to manage sensor driven and fusion, attitude and position control, and communication with onboard PC. The PC, Up-board installed with Linux operating system including ROS [16], which is responsible for receiving pose information from VICON, and processing flight planning commands. The overview of the quadrotor system architecture is shown in Fig. 3.

B. Filter Performance Validation

In flight experiments, each of the designed aggressive maneuvers lasts 90 to 120 seconds, and is conducted more than 15 times. During any maneuver, the proposed filter with EKF and ESKF for comparison is performed simultaneously. Meanwhile, the orientation results of three tested filters and VICON, in format of quaternion are recorded. To ensure the uniformity of data structure, we record all the raw MARG sensors data in rosbags and build an individual data process node in ROS. By collecting filter outputs in this node, we align them in the same time stamp, which is necessary for realtime comparison and subsequent calculation. Based on the aligned comparison, we use the root mean squared error (RMSE) to evaluate estimate accuracy, and utilize the runtime of every algorithm epoch to evaluate estimate efficiency. The experiment of realtime aggressive maneuvers, including flight path depicting and quadrotor orientation output, is shown in the attached video.

1) Two-point loop maneuver: We randomly preplan two cartesian points in the world reference frame. The quadrotor is commanded to move from one point to the other one, with initial large inclination angles. The loop motion is consecutive. Fig. 4 extracts the period of two-point loop motion, from $30s$ to $60s$. It could be seen that, the largest rotation Euler angle: Roll is more than 50^o.

2) Two-triangle loop maneuver: The aim is to test filters' performance, when both pitch and roll angles of quadrotor's attitude are violently changing. We set five cartesian points, which form two triangles. The quadrotor moves in a fixed direction, following the five points. Also, Fig. 5 shows $30s$ of the two-triangle loop flight. The flight covers large variety of both pitch and roll angles, which leads to more flight attitudes of the quadrotor.

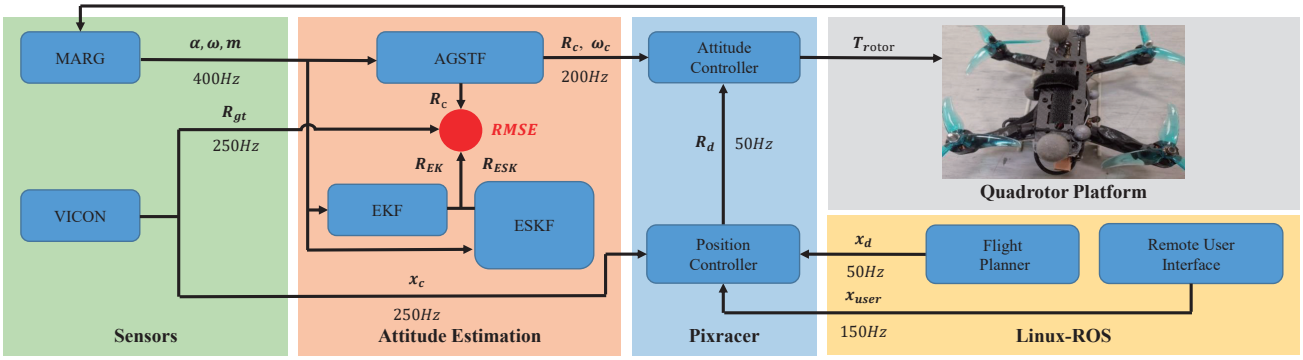

Fig. 3. Overview of the quadrotor system setup. Sensors block includes MARG sensors which provide acceleration, magnetic fields and angular rates. Attitude estimation block covers the proposed filter with two compared filters: EKF and ESKF. Pixracer block executes flight control, with receiving planning command from Linux-ROS block.

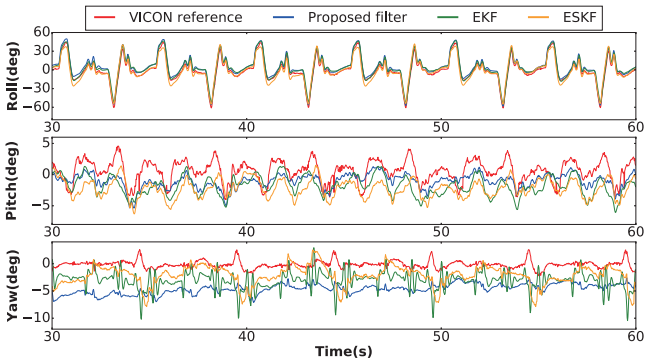

Fig. 4. Orientation comparison results of the two-point loop flight. The orientation is in format of Euler angles: **RPY**.

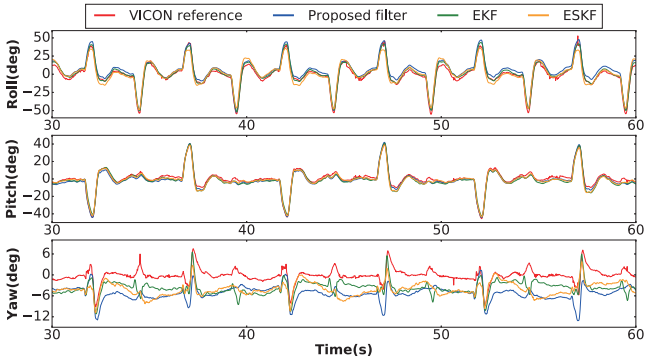

Fig. 5. Orientation comparison results of the two-triangle loop flight.

3) Fixed-point rotation maneuver: During the flight, we manipulate the extent of aggressive rotation by setting the yaw angular rate. The goal of this designed maneuver is to test the performance of yaw angle estimate, in aggressive self-rotation. In Fig. 6, ESKF outputs in pitch and roll angles, perform apparent oscillation, while the proposed filter and EKF have good estimate.

According to estimation results of Euler angles, we compute RMSE of each performed filter in each maneuver. The RMSE results including Euler angles: **RPY** show as Table. I. It can be investigated that the proposed filter perform

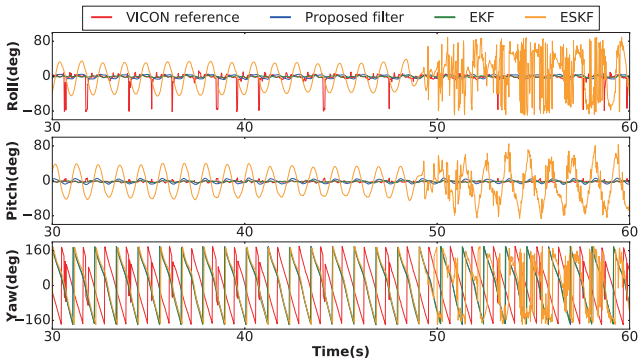

Fig. 6. Orientation comparison results of the fixed-point rotation flight.

the best during maneuvers with large change in pitch and roll angles. Meanwhile, the proposed filter and EKF have better performance in aggressive rotation flights. As for filter estimate efficiency, we record 500 consecutive and simultaneous epochs of the above algorithms.

TABLE I
RMSE COMPARISON RESULTS

Maneuvers	Attitude (°)	**AGSTF**	EKF	ESKF
Two-point	pitch	**2.132°**	2.757°	2.809°
	roll	**3.357°**	4.711°	4.824°
	yaw	4.567°	4.848°	**4.560°**
Two-triangle	pitch	**2.131°**	2.862°	2.257°
	roll	**3.273°**	3.984°	4.446°
	yaw	8.416°	**8.180°**	8.247°
Fixed-point	pitch	3.461°	**3.033°**	29.586°
	roll	11.749°	**11.340°**	35.001°
	yaw	**15.250°**	17.186°	19.551°

° represents the degree of Euler angles.
AGSTF denotes the proposed filter.

The comparison result is shown in Fig. 8, where both EKF and ESKF consume nearly 100 times more time than the proposed filter. Also, the overall runtime of the proposed filter reaches higher stability than others. Fig. 7 shows the actual experiment of three designed aggressive maneuvers,

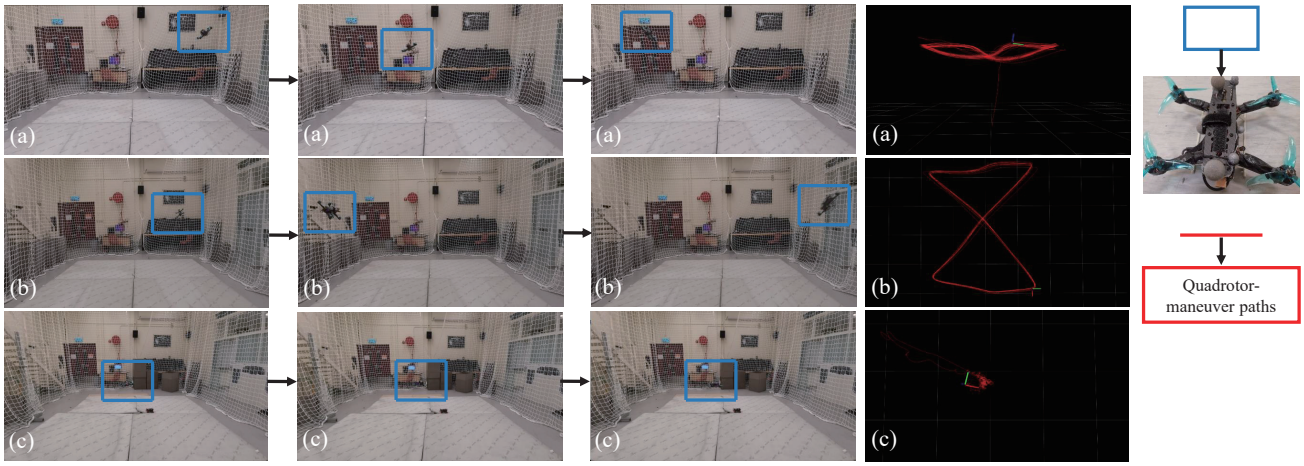

Fig. 7. Actual experiment flight of the proposed quadrotor platform. (a) Two-point loop flight (front view). (b) Two-triangle loop flight (bird view). (c) Fixed-point rotation flight (bird view).

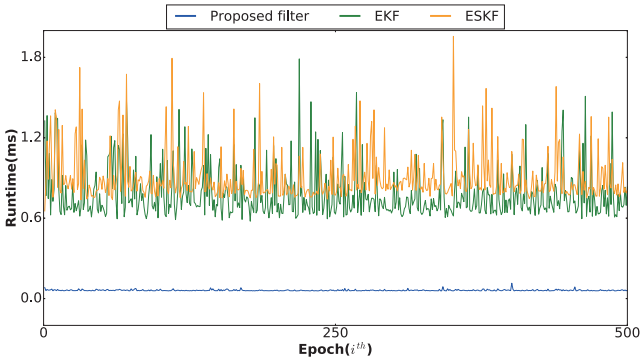

Fig. 8. Algorithm runtime results of 500 epochs for the proposed filter, EKF and ESKF.

including several scenes and complete flight paths.

V. Conclusion

In this paper, we propose an adaptive Complementary Filter for aggressive maneuvers of a quadrotor. With adaptivity to the extent of maneuvers, the proposed CF fuse acceleration, magnetic field and angular velocity from a MARG sensor system. To validate the performance, we establish a light-weight quadrotor and a flight field with VICON system. In flight experiments, the quadrotor utilizes the estimated attitude from the proposed CF, and conducts simultaneous comparison with EKF and ESKF. Results show that, the CF outperforms in both accuracy and efficiency of the fast attitude estimate, during the quadrotor's aggressive maneuvers.

References

[1] G. Loianno, C. Brunner, G. McGrath, and V. Kumar, "Estimation, control, and planning for aggressive flight with a small quadrotor with a single camera and imu," *IEEE Robotics and Automation Letters*, vol. 2, no. 2, pp. 404–411, 2016.

[2] D. Mellinger, N. Michael, and V. Kumar, "Trajectory generation and control for precise aggressive maneuvers with quadrotors," *The International Journal of Robotics Research*, vol. 31, no. 5, pp. 664–674, 2012.

[3] S. Liu, K. Mohta, N. Atanasov, and V. Kumar, "Search-based motion planning for aggressive flight in se (3)," *IEEE Robotics and Automation Letters*, vol. 3, no. 3, pp. 2439–2446, 2018.

[4] S. Tang, V. Wüest, and V. Kumar, "Aggressive flight with suspended payloads using vision-based control," *IEEE Robotics and Automation Letters*, vol. 3, no. 2, pp. 1152–1159, 2018.

[5] A. Bry, A. Bachrach, and N. Roy, "State estimation for aggressive flight in gps-denied environments using onboard sensing," in *2012 IEEE International Conference on Robotics and Automation*. IEEE, 2012, pp. 1–8.

[6] J. Thomas, M. Pope, G. Loianno, E. W. Hawkes, M. A. Estrada, H. Jiang, M. R. Cutkosky, and V. Kumar, "Aggressive flight with quadrotors for perching on inclined surfaces," *Journal of Mechanisms and Robotics*, vol. 8, no. 5, 2016.

[7] M. Watterson and V. Kumar, "Safe receding horizon control for aggressive mav flight with limited range sensing," in *2015 IEEE/RSJ International Conference on Intelligent Robots and Systems (IROS)*. IEEE, 2015, pp. 3235–3240.

[8] S. O. Madgwick, A. J. Harrison, and R. Vaidyanathan, "Estimation of imu and marg orientation using a gradient descent algorithm," in *2011 IEEE international conference on rehabilitation robotics*. IEEE, 2011, pp. 1–7.

[9] R. Mahony, T. Hamel, and J.-M. Pflimlin, "Nonlinear complementary filters on the special orthogonal group," *IEEE Transactions on automatic control*, vol. 53, no. 5, pp. 1203–1218, 2008.

[10] H. G. De Marina, F. J. Pereda, J. M. Giron-Sierra, and F. Espinosa, "Uav attitude estimation using unscented kalman filter and triad," *IEEE Transactions on Industrial Electronics*, vol. 59, no. 11, pp. 4465–4474, 2011.

[11] S. Guo, J. Wu, Z. Wang, and J. Qian, "Novel marg-sensor orientation estimation algorithm using fast kalman filter," *Journal of Sensors*, vol. 2017, 2017.

[12] M. Xu, N. Fan, and Z. Wang, "Study on extended kalman filtering for attitude estimation of micro flight vehicle," in *2011 Third International Conference on Measuring Technology and Mechatronics Automation*, vol. 3. IEEE, 2011, pp. 457–460.

[13] J. Sola, "Quaternion kinematics for the error-state kalman filter," *arXiv preprint arXiv:1711.02508*, 2017.

[14] N. B. da Silva, D. B. Wilson, and K. R. Branco, "Performance evaluation of the extended kalman filter and unscented kalman filter," in *2015 International Conference on Unmanned Aircraft Systems (ICUAS)*. IEEE, 2015, pp. 733–741.

[15] V. Madyastha, V. Ravindra, S. Mallikarjunan, and A. Goyal, "Extended kalman filter vs. error state kalman filter for aircraft attitude estimation," in *AIAA Guidance, Navigation, and Control Conference*, 2011, p. 6615.

[16] M. Quigley, K. Conley, B. Gerkey, J. Faust, T. Foote, J. Leibs, R. Wheeler, and A. Y. Ng, "Ros: an open-source robot operating system," in *ICRA workshop on open source software*, vol. 3, no. 3.2. Kobe, Japan, 2009, p. 5.